Nanoscale Advances

ROYAL SOCIETY OF CHEMISTRY

PAPER

View Article Online
View Journal | View Issue

Cite this: *Nanoscale Adv.*, 2022, **4**, 4606

Effect of a layer-by-layer assembled ultra-thin film on the solid electrolyte and Li interface

Nurbol Tolganbek,[a] Madina Sarsembina,[a] Arailym Nurpeissova,[b] Kiyoshi Kanamura,[c] Zhumabay Bakenov *[ab] and Almagul Mentbayeva *[a]

Advanced all-solid-state batteries are considered as the most preferable power source for the next generation devices. Such batteries demand consumption of electrode materials with high energy and power density. One of the excellent solutions is the utilization of Li metal as anode which provides opportunity to fulfill such requirements. Yet, obstacles such as interfacial impedance and reactivity of Li metal with promising solid electrolytes prevent the consumption of the Li anode. Despite its outstanding stability under ambient conditions, high ionic conductivity and facile synthesis methods, NASICON-type $Li_{1.3}Al_{0.3}Ti_{1.7}(PO_4)_3$ also suffers from the above mentioned problems. In this work, these critical issues were resolved by applying an artificial protective interlayer. Herein, the layer-by-layer polymer assembly approach of the ultra-thin interlayer of $(PAA/PEO)_{30}$ on either side of solid electrolyte pellets simultaneously is presented. The introduction of the protective layer prevented a formation of mixed conduction interphase and effectively decreased the interfacial impedance. A symmetric cell with Li metal electrodes performed over 600 hours at 0.1 mA cm^{-2}. Furthermore, an all-solid-state Li metal battery, assembled with the modified LATP solid electrolyte and $LiFePO_4$ cathode, demonstrated an excellent electrochemical performance with an initial discharge capacity of 115 mA h g^{-1} and a capacity retention of 93% over 20 cycles with a coloumbic efficiency of almost 100%. The LATP with the $(PAA/PEO)_{30}$ coating exhibited electrochemical stability up to 5 V.

Received 5th August 2022
Accepted 9th September 2022

DOI: 10.1039/d2na00521b

rsc.li/nanoscale-advances

Introduction

Next generation batteries with prolonged cyclability, high energy density, safety and reliability along with a high operating potential are required to meet the performance properties of new devices and applications for further progress in portable electronics, ecological transport, communication devices and many other areas.[1–7] Along with high performance electrode materials, such advances of Li-ion and Li metal batteries mainly depend on the development of new types of solid ion conductors to replace commercial liquid electrolytes.[8–13] Despite the admirable benefits of commercial liquid ion conductors, these electrolytes have been facing dramatic safety problems and an inability to operate above certain potentials and at elevated temperatures causing their decomposition and fire.[14–16] These problems are worsened further due to their potential leakage and reaction with the electrode materials. On top of all these dramatic problems, incompatibility of lithium metal and liquid electrolytes due to uneven deposition of lithium causing dendrite growth, raises another big issue.[17–20] Thus, new types of solid electrolytes should be developed to address these issues along with possessing high ionic conductivity, chemical and mechanical stability and simple handling. To date, potential candidates that satisfy most of these requirements are polymer and/or inorganic electrolytes. Solid electrolytes based on inorganic materials have gained popularity due to their safe operation, and sufficient ionic conductivity.[18,21] Currently there are several types of solid inorganic electrolytes available, namely argyrodite, garnet, Li-nitride, Li-halide, Li-hydride, perovskite, LISICON and NASICON.[22–31] Among them, the last mentioned ceramic material caught attention because of its stability towards air and moisture under ambient conditions.[32–34] Superior stability and a high ionic conductivity of 10^{-4} to 10^{-3} S cm^{-2} at room temperature enabled the material to be the most suitable candidate for an all-solid-state battery.[21,25,35,36] Particularly, the composition $Li_{1.3}Al_{0.3}Ti_{1.7}(PO_4)_3$ (LATP) demonstrated the most promising results. Within some doping limits, an aluminum dopant (Al^{3+}) allows the accommodation of more lithium in interstitials to compensate for the charge balance; however, a dopant amount above 0.3 led to the formation of an undesired impurity phase of $AlPO_4$.[32,37,38] LATP ceramics can be fabricated through different synthesis routes depending on the requirements regarding the shape and size of particles.[39–48] Despite all these compelling advantages, LATP cannot tolerate

[a]*School of Engineering and Digital Sciences, Nazarbayev University, Nur-Sultan, Kazakhstan. E-mail: almagul.mentbayeva@nu.edu.kz*

[b]*National Laboratory Astana, Nazarbayev University, Nur-Sultan, Kazakhstan. E-mail: zbakenov@nu.edu.kz*

[c]*Tokyo Metropolitan University, Tokyo, Japan*

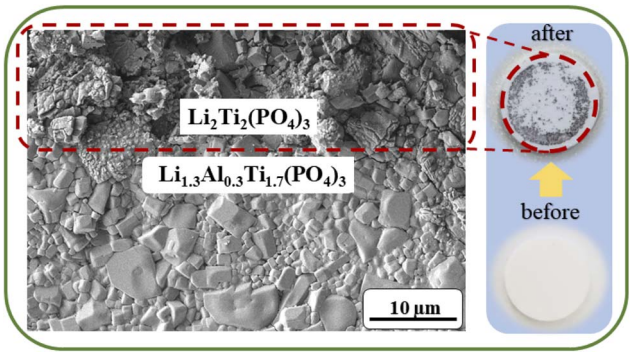

Fig. 1 SEM image and visual illustration of the MCI.

direct contact with lithium metal.[49–60] There is an abrupt reduction process happening, where Ti^{4+} reduces to Ti^{3+} forming a secondary phase of a mixed conducting interphase (Fig. 1) that hinders lithium-ion conduction but facilitates the electron conduction.[61–78]

This issue can be resolved by applying a protective layer of lithium ion conducting substances. The most recent studies addressing this problem include deposition of artificial layers based on inorganic substances such as oxides, lithium salts, nanocomposites and other types of lithium conducting solid materials.[79] Liu *et al.* introduced Al_2O_3 and Li_3PO_4 materials as interface stabilizers using atomic layer deposition (ALD), while Bai *et al.* suggested depositing an Al_2O_3 doped ZnO layer on LATP using a magnetron sputtering tool.[42,60] Cheng *et al.* protected LATP by depositing boron nitride nanocomposites *via* chemical vapor deposition (CVD).[59] In these studies, LATP was physically protected from direct contact with Li metal. Nonetheless, this kind of material requires certain deposition techniques as well as inert atmosphere conditions and these processes are time consuming and not cost effective. Other perspective approaches involve polymer electrolyte films on LATP or combining polymers with ceramics creating composite electrolytes. Yi *et al.* investigated a hybrid electrolyte of poly(vinylidene fluoride) (PVdF), poly(ethylene oxide) (PEO) and LATP.[56] Shi *et al.* fabricated a LATP and PVdF composite electrolyte.[52] Yet, all these systems achieved improved electrochemical performance consuming a large amount of liquid electrolytes. There are also some studies that report coating the surface of LATP with lithium ion conducting polymers, mostly PEO, which has insufficient ionic conductivity at room temperature. The thicknesses of these interlayers were from 10 to 100 micron and usually a thick film negatively affects charge transfer capability, creating additional barriers for lithium ion migration. Overall, the up-to-date status of various interlayers LATP and LAGP with the results of Li stripping and plating performance duration is depicted in Fig. 2.[79]

It can clearly be seen that the interlayers designed from inorganic substances only operate at very low current densities, while the polymers showed very stable performance at higher current densities. It can be concluded from Fig. 2 that further developments on the solid electrolyte and Li metal interface are preferable to be carried out by utilizing artificial interlayers made of lithium ion conducting polymer materials.[79]

Therefore, in this report, we propose a 65–75 nm artificial interlayer of $(PAA/PEO)_{30}$ through the layer-by-layer (lbl) assembly technique between LATP and Li metal to prevent mixed conduction interphase (MCI) formation and to decrease the interface impedance as well. The lbl polymer coating method enabled achieving an ultra-thin texture with precise thickness control by manipulating the insertion numbers. A symmetric cell with Li non-blocking electrodes operated over 600 hours with a very low overpotential response as well as electrochemical stability up to 5 V. Furthermore, a simultaneous polymer coating on both sides of LATP also improved the interface between the cathode and solid electrolyte resulting in significantly enhanced performance of an all-solid-state Li battery (ASSLB). The ASSLB with a commercial olivine $LiFePO_4$ cathode displayed a highly reversible electrochemical behavior with an initial discharge capacity of 115 mA h g^{-1} and coloumbic efficiency of about 100%.

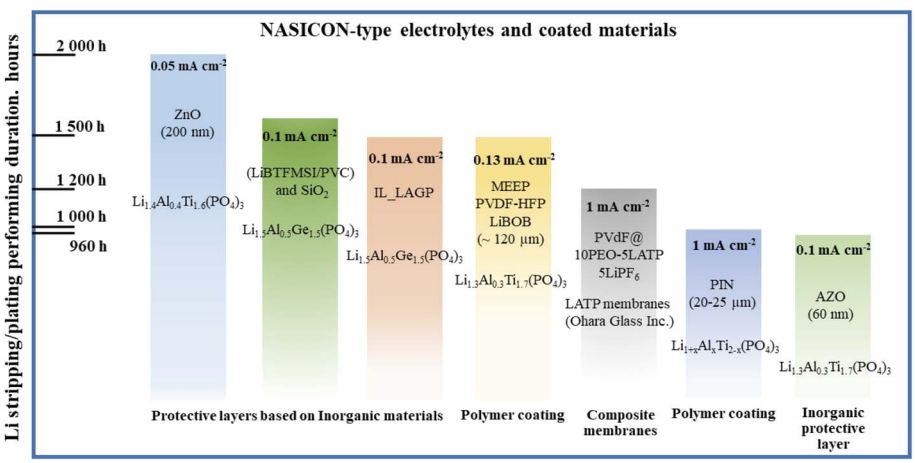

Fig. 2 Status of artificial layers on NASICON-type LATP and LAGP solid electrolytes.[79]

Experimental section

Preparation of LATP solid electrolyte

$Li_{1.3}Al_{0.3}Ti_{1.7}(PO_4)_3$ ceramic material was fabricated *via* the molten flux method. The procedure was slightly modified where a flux ($CO(NH_2)_2$) was first dissolved in deionized water (DIW). Then, water soluble chemicals such as $LiNO_3$ (98%) and $NH_4H_2PO_4$ (98%) were added in a stoichiometric ratio. The remaining insoluble components, Al_2O_3 and TiO_2, were introduced into the solution after 10 minutes of mixing. The mixture was stirred for 4 hours and dried at 120 °C for 12 hours. The solid residue then was crushed in an agate mortar and heated at 500 °C for 8 hours. The resulting powder was mixed in a ball-mill at 450 rpm for 4 hours in acetone (Pulverisette, FRITSCH, ZrO_2 ball, 6 mm in diameter). The ball-milled powder was pelletized with an 8 mm die and calcined at 900 °C for 6 hours in air in a muffle furnace (ELF 11/6B, Carbolite Gero Ltd.). To mitigate the evaporation/loss of lithium during high temperature calcination, an extra 5% lithium salt was added while preparing the solution.

Preparation of aqueous polymer solutions

Branched poly(ethylenimine) (PEI; MW = 750 000, 50 wt% in H_2O), poly(ethylene oxide) (PEO; MW = 100 000), and poly(-acrylic acid) (PAA; MW = 450 000) were used as received and dissolved in deionized water with a concentration of 0.2 g dm^{-3}. The pH values of polymer solutions were 6 and 2.6 for PEI and PAA, PEO, respectively. Adjustments of pH were carried out by using diluted HCl and NaOH solutions.

Layer-by-layer assembly of polymers

The lbl process was carried out using a dip coating robot DR-3 (Riegler & Kirstein GmbH) by programming insertion processes. Prior to the coating procedure, pellets of LATP were treated with 5% of H_2O_2 to create charge on the surface and then rinsed in DI water. Then, the pelletized samples were immersed in a positively charged solution of PEI for 5 minutes to form a precursor layer. Next, the pellets were dipped in PAA and PEO solutions with a pH of 2.6 for 5 minutes and washed with 0.01 M Trizma® buffer solution with the same acidity (Fig. 3). Alternate insertion of pellets into these polymer solutions was assigned as $(PAA/PEO)_n$ and the process was carried out for 30 times with the final composition of $(PAA/PEO)_{30}$.

Characterization techniques

The structure and morphology of the synthesized and $(PAA/PEO)_{30}$ coated LATP were investigated by using an X-ray diffractometer (XRD, Rigaku SmartLab XRD system) equipped with a Cu X-ray tube, a D-Tex detector and a scanning electron microscope (SEM, Crossbeam 540, FeSEM Auriga). The thickness of the layer was measured using an ellipsometer (SENresearch 4.0, Sentech) and the polymers were coated on one side of a polished Si wafer.

Electrochemical characterization techniques

Prior to electrochemical measurements, the $LiPF_6$ commercial liquid electrolyte (0.5 μl) was dropped onto a thin polymer layer as a Li-ion source for ion conduction. Electrochemical impedance spectroscopy (EIS) using lithium (non-blocking) electrodes in a frequency range of 1 Hz to 1 MHz (potentiostat/galvanostat, Metrohm AutoLab 204) was used to measure the ionic conductivity. A continuous stripping and plating test of Li-ions in symmetric cells with lithium metal electrodes was carried out by using a potentiostat/galvanostat (Bio-Logic SAS VMP3) at 0.1 mA cm^{-2} current density. Linear sweep voltammetry (LSV) was conducted using a potentiostat–galvanostat (VMP3, Bio-Logic Inc.) between −0.5 to 5.5 V using blocking (stainless steel, SS) and non-blocking (lithium metal) electrodes. A full all-solid-state Li metal battery was assembled and investigated by cyclic voltammetry (CV) and galvanostatic charge/discharge tests. $LiFePO_4$ (LFP) olivine-type commercial material was used as the cathode. All cells were prepared using polished pristine and $(PAA/PEO)_{30}$ coated LATP pellets.

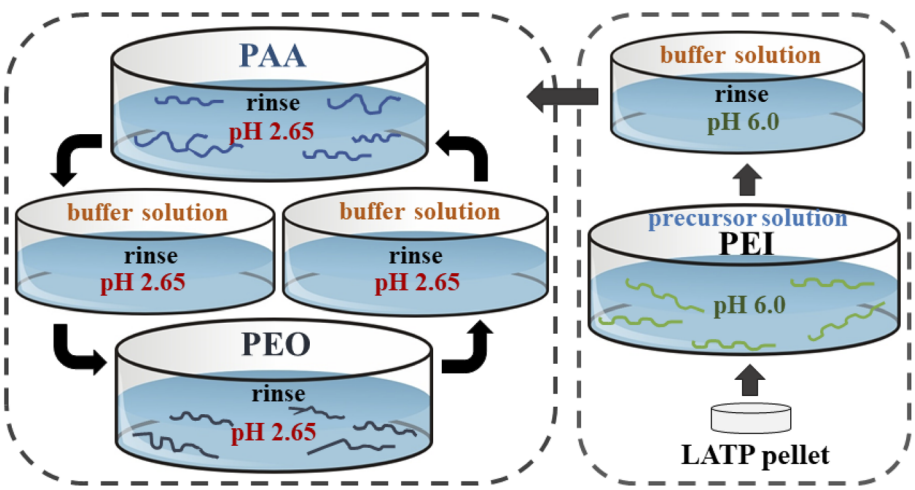

Fig. 3 Visual illustration of the lbl assembly process on LATP pellets.

Results and discussion

The elementary molten flux preparation method demonstrated that single phase LATP can be fabricated without any impurities. Introduction of the flux, additional lithium inclusion and optimal calcination temperature not exceeding 900 °C facilitated production of pure LATP ceramic which was confirmed *via* an X-ray diffractometer. The synthesized powder had a rhombohedral structure with a $R\bar{3}c$ space group. This again confirms the importance of the synthesis method and its parameters we discussed in the earlier work.[80] Furthermore, for the advancement of the solid electrolyte/electrode interface and to protect LATP from reduction by Li metal, the ceramic pellets were successfully coated with ultra-thin (PAA/PEO) multilayers by the lbl technique. This was achieved by creating a negatively charged surface by treating the pellets with H_2O_2, and this facilitated the adhesion of positively charged PEI on LATP as a precursor layer. It was followed by deposition of a negatively charged PAA layer to form a strong electrostatically bonded initial bilayer with the composition of (PEI/PAA) (Fig. 4a). Generally, the thin layer consists of two main polymers of PAA and PEO, and the samples were dip coated consequently for 5 minutes.

The lbl assembly was carried out using polymer solutions with pH 2.65. Following each polymer deposition step, the LATP pellets were washed with Trizma® buffer solution (0.01 M) with the same pH for 2 minutes. Completion of (PAA/PEO) insertions was considered to be one bilayer (bl) and the dipping procedure was repeated 30 times (30 bls). Initially, the link between PAA and PEO is based on intermolecular hydrogen bonding as illustrated in Fig. 4a. The structural stability of the ceramic after continuous immersion in mild acidic solutions was also validated by XRD after the lbl coating technique. Fig. 4b depicts the XRD patterns of the samples and shows that the structure of LATP did not change upon the treatments, proving chemical durability of the ceramic material. Afterwards, heating at 130 °C enabled transition of the intermolecular forces such as electrostatic and hydrogen bonds to covalent bonds, precisely, and PEI and PAA links through amine and carboxylic groups while PAA and PEO, through carboxylic and terminal groups as previously reported.[81–83] Despite the thinness, the polymer coating provided high durability and cohesion due to the covalent bonding. The mechanical stability and ionic conductivity of the $(PEO/PAA)_n$ thin film as solid polymer thin film electrolyte was examined by Hamedi *et al.*[83] It was found that a cross-linked texture had mostly an amorphous phase, which greatly favored high lithium ion conduction achieving $2.3 \pm 0.8 \times 10^{-4}$ S cm^{-1}.[83]

The SEM image of pristine LATP revealed that particles have a cubic shape with a grain size of up to ~9 μm (Fig. 5a). A previous report clearly showed that well-defined cubic shape LATP particles with larger crystals are more favorable due to their high compactness. Onwards, the lbl assembled polymer on LATP image from the top view is depicted in Fig. 5b.[80] The lbl coating technique enabled obtaining an ultra-thin and uniform texture that covered the whole surface of a pellet without any breach (Fig. 5b). The growth of the nanofilm was also followed by ellipsometry when the cleaned and polished Si wafer was utilized as a substrate. The thickness of the first PEI layer was estimated to be 1.7 ± 0.2 nm, while the (PAA/PEO) bilayer had a thickness of 2.5 ± 0.5 nm which increased linearly with the bilayer numbers. The final thickness of the polymer interlayer was estimated to be between 65 and 75 nm, which is also well matched with a value from SEM cross-sectional image (Fig. 5c).

Prior to the electrochemical performance studies, the LATP pellets were visually tested for the reactivity with the negative electrode of the Li metal disc by making them come into contact. The results certainly indicated the formation of an MCI on top of pristine LATP. Zhu *et al.* believed that the MCI began to form between the electrolyte and electrode interface during the lithiation process.[84] However, our examination clearly demonstrated that the reaction between LATP and Li metal proceeds instantly when they came into contact, as both components are highly reactive. Evidently, the experiment confirmed the instant reduction of LATP while in contact with Li metal (Fig. 6). This reaction creates obstacles to combining this electrolyte with Li metal, which restricts its consumption in Li batteries. Apparently, the pellet with a protective layer demonstrated durability towards Li metal even after 24 hours of physical contact.

In the nick of time, this side reaction can be prevented by an artificial buffer layer of $(PAA/PEO)_{30}$. This physical barrier not

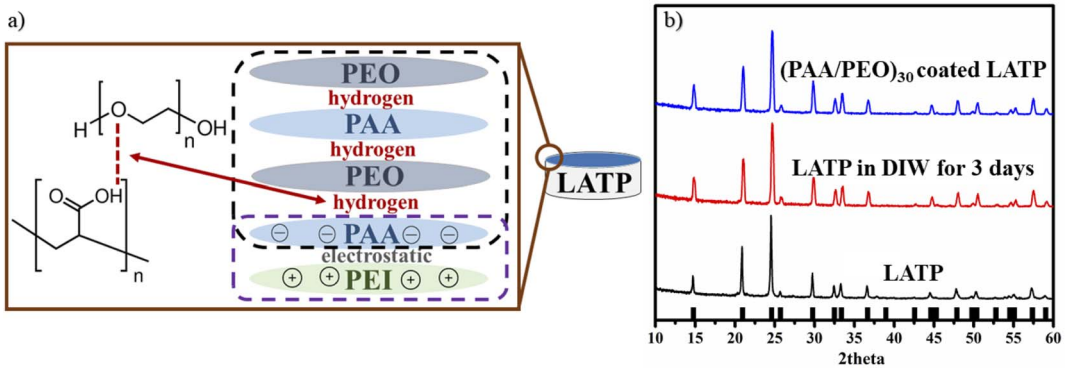

Fig. 4 (a) Film growth mechanism between polymers and (b) the XRD pattern of pristine, deionized water treated and $(PAA/PEO)_{30}$ coated LATP.

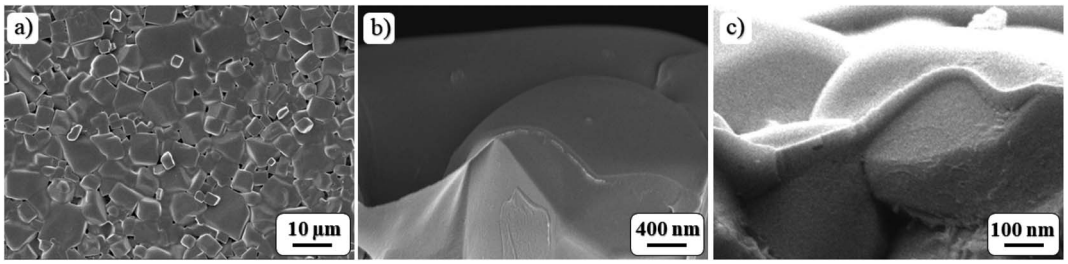

Fig. 5 SEM images, (a) top and (b and c) cross sectional views of $(PAA/PEO)_{30}$ coated LATP pellets.

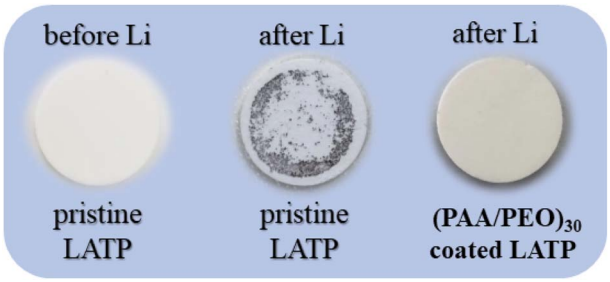

Fig. 6 Visual test for pristine and modified LATP with Li metal.

only hinders the direct contact between LATP and Li metal preventing their reaction, but it also allows high lithium-ion transfer through its matrix. Besides, the protective interlayer was one of the most efficient approaches towards decreasing the interfacial impedance between the solid electrolyte and electrodes. The current work was not an exception, as this very thin interlayer designed from polymer material created soft intermedia for these two materials by providing a continuous path for Li-ion migration. This also positively influences the overall kinetics of charge transfer and the electrochemical reaction.

Further electrochemical studies were conducted with pristine and $(PAA/PEO)_{30}$ coated LATP. The ionic conductivity measurements of different cell configurations were conducted in a cell with Li metal non-blocking electrodes and the electrolytes sandwiched between them. The electrochemical impedance spectrum of sandwiched polished pristine LATP with Li electrodes is obviously depicting a large charge transfer resistance due to the reduction of the ceramic electrolyte and formation of an MCI (Fig. 7a). As an extension of this, a lack of confined contact of surfaces between LATP and Li metal also contributed to high impedance. In contrast, the LATP pellet with a $(PAA/PEO)_{30}$ film showed a lower interfacial impedance with a charge transfer resistance two times smaller than that for the pristine LATP sample, resulting from a smooth transfer of Li-ions through the electrolyte to the electrode (Fig. 7a) by the provided profound contact with the interlayer. The ionic conductivity of Li/LATP/Li and Li/$(PAA/PEO)_{30}$/LATP/$(PAA/PEO)_{30}$/Li, systems were 1.8×10^{-5} S cm^{-1} and 1.6×10^{-4} S cm^{-1}, respectively, demonstrating that the use of the interlayer allows a conductivity of one order higher to be achieved. Along with protection from the side reaction, this layer provided definite connection without limiting Li-ion transfer[85,86]. In both cases, the Warburg impedance was not observed in a lower frequency region due to the non-blocking electrode's nature. An identical cell configuration was also tested for thw stripping and plating test at 0.1 mA cm^{-2} (Fig. 7b). As the results show, the Li/LATP/Li system operates for only around 40 hours with a very large overpotential response. Abrupt decline in resistivity that could be seen from the potential response data is related to the interface degradation leading to a large electrolyte/electrode interface impedance between the electrolyte and electrode.

The introduction of an artificial interlayer enabled the formation of a lithium-deficient layer for interdiffusion that significantly improved the interfaces as $(PAA/PEO)_{30}$ was coated on both sides of LATP simultaneously. The Li/$(PAA/PEO)_{30}$/

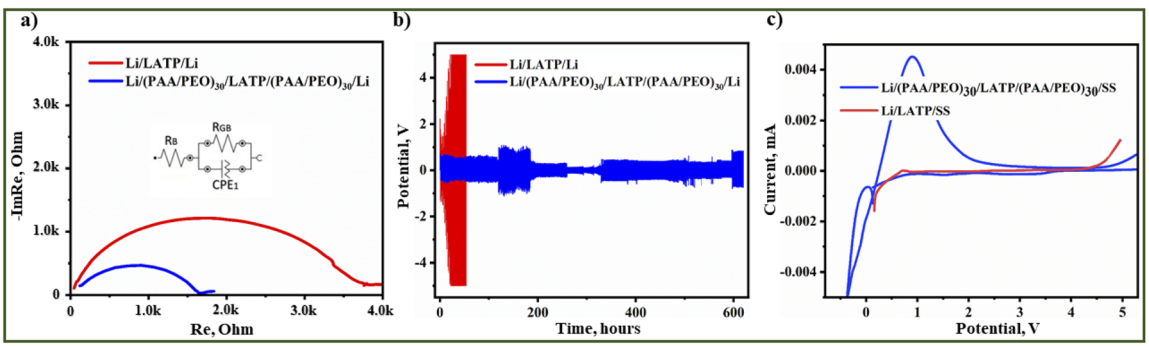

Fig. 7 Results of electrochemical performance of pristine and $(PAA/PEO)_{30}$ coated LATP pellets; (a) EIS spectra; (b) stripping and plating behavior; (c) LSV profile.

LATP/$(PAA/PEO)_{30}$/Li cell exhibited 600 hours of cyclability with the lowest overpotential response (−1 to 1 V) (Fig. 7b). Due to the formation of intrinsic resistivity, the cell showed a slightly higher potential response for about 50 hours, and further stabilized with even lower response. Still, the cell depicted some resistivity after 600 hours due to intrinsic microstructural fractures which could be explained by chemomechanical stress. The cells with configurations such as SS/LATP/Li and SS/$(PAA/PEO)_{30}$/LATP/$(PAA/PEO)_{30}$/Li were assembled for the electrochemical stability measurements by linear sweep voltammetry (LSV) in a potential range of −1 to 5.5 V with a scanning rate of 0.1 mV s^{-1}. According to the obtained voltammograms lithium intercalation and deintercalation are significantly well defined in LATP with a polymer coating while peaks related to these reactions are negligible in the pristine sample. In addition, the cell with bare LATP has electrochemical stability up to 4.4 V (Fig. 7c) while the modified LATP with a $(PAA/PEO)_{30}$ coating was stable up to 5 V with slow decomposition at a potential exceeding 5 V (Fig. 7c). Furthermore, this promising feature of the advanced polymer coated LATP solid electrolyte was further examined in the all-solid-state Li metal battery (ASSLB) with a commercial olivine structured $LiFePO_4$ (LFP) cathode. The cathode composite casting was carried out in a non-traditional way by brush painting a cathode slurry with a composition of LFP : AB : PVdF in a ratio of 65 : 20 : 15 (weight) on well-polished pristine and $(PAA/PEO)_{30}$ coated LATP. This method of applying the electrode and a high amount of PVdF was chosen to enhance the cathode adhesion on the surface of the electrolyte pellets. We compared this technique with the traditional doctor-blade method of casting a cathode on the Al current collector but it did not show any electrochemical response due to the lack of proper contact between the electrode and electrolyte. In contrast, our painting technique allowed very reproducible high performance data to be obtained for our polymer coated LATP electrolyte.

Two ASSLB systems, namely, Li/LATP/LFP and Li/$(PAA/PEO)_{30}$/LATP/$(PAA/PEO)_{30}$/LFP with the addition of 0.5 μl commercial liquid electrolyte to wet the polymer matrix for lithium ion transport, were assembled in an inert atmosphere glovebox. Prior to cycling, the EIS technique was applied to examine the overall resistivity of the cell. The ASSLB with bare LATP had the highest resistivity due to the known reasons of the reduction side reaction (Fig. 8a). In contrast, the lowest resistivity of the modified electrolyte pellets was because of a thin polymer layer with Li-salt in it. The role of the liquid electrolyte in the performance of solid electrolyte also was tested, and the results revealed that wetting bare LATP does not aid in decreasing the charge transfer resistance as its resistivity was still higher than that of with the polymer film (Fig. 8a). Next, the CV measurements showed the reversible reactions related to the redox process of LFP, but with high polarization due to poor kinetics and the presence of accompanying resistivity mostly within the ceramic electrolyte (Fig. 8b). The CV profile of Li/LATP/LFP demonstrated a weak response to the oxidation

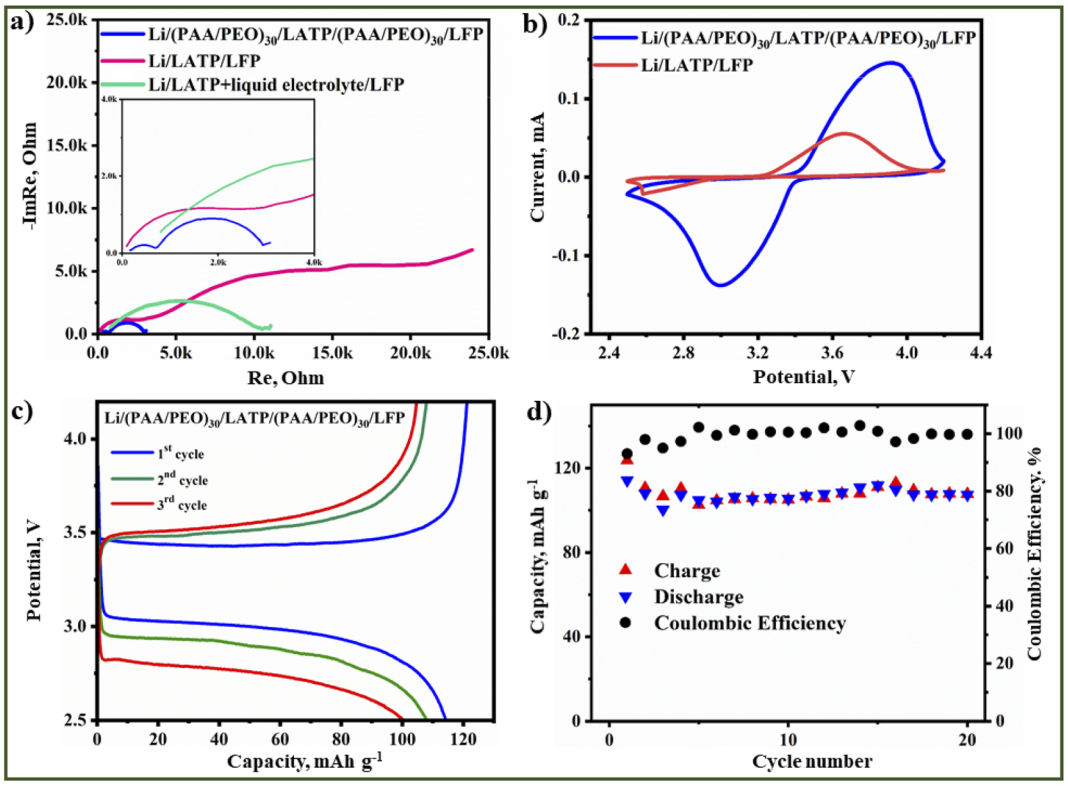

Fig. 8 Results of electrochemical performance of the ASSLB with pristine and $(PAA/PEO)_{30}$ coated LATP pellets: (a) EIS spectra; (b) CV and (c) galvanostatic charge and discharge profiles; (d) cyclability and coulombic efficiency.

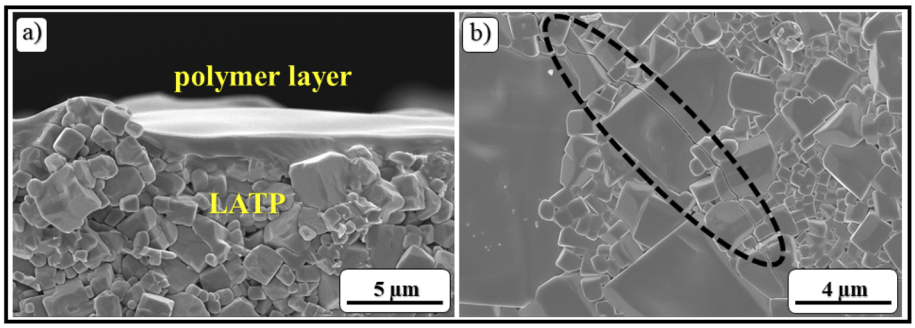

Fig. 9 SEM images of a disassembled ASSLB with a $(PAA/PEO)_{30}$ film after 20 cycles; (a) cross-section of LATP and $(PAA/PEO)_{30}$; (b) fracture of LATP grains.

process of the cathode material, and the reduction process was not equivalent, which is due to the lithium ion blocking in the interface caused by a side reaction of Li metal with LATP. In the case of LATP with a polymer film, it exhibited very intense reversible peaks related to the redox of LFP. An ASSLB with polymer texture performed 20 cycles at 0.1C with an initial discharge capacity of 115 mA h g^{-1} and a coulombic efficiency of 93% (Fig. 8c and d). In the subsequent cycles, the coulombic efficiency increased to 100% with stable discharge capacities from 107 to 102 mA h g^{-1}.

The morphology of LATP and the polymer film after 20 charge–discharge cycles was observed by using the SEM images (Fig. 9). The cross-sectional image in Fig. 9a clearly shows that the film has not changed maintaining its uniformity. However, other observations revealed that the ceramic grains have large fractures of different sizes from 10 to 200 μm. The limited operation of the ASSLB could be explained by these fractures that occurred because of chemomechanical stress upon cycling. This kind of outcome was found in many reports on solid electrolyte research.[85–98] Regardless of the chemomechanical fractures, the lbl assembled ultra-thin polymer significantly improved the interfaces in a solid-state cell and conserved its morphology and uniformity over 20 galvanostatic charge discharge cycles. Importantly, the formation of the MCI layer was not observed for this system which was confirmed by the cross-section image in Fig. 9a.

Conclusion

The research presented a thin artificial protective texture of $(PAA/PEO)_{30}$ as an interlayer between LATP and Li metal through the layer-by-layer polymer assembly technique. Firstly, the ultra-thin interlayer assisted in preventing the formation of the mixed conductive interphase. Secondly, the artificial polymer texture decreased the interfacial impedance at the electrolyte/electrode border by providing intimate contact between solid electrolyte and electrodes for non-disruptive lithium ion insertion and extraction for 600 hours at 0.1 mA cm^{-2}. Thirdly, simultaneous polymer coating on both sides of the LATP pellets enabled the design of an all-solid-state Li metal battery with a commercial LFP cathode that demonstrated a highly reversible electrochemical behavior.

Conflicts of interest

There are no conflicts to declare.

Acknowledgements

This research was supported by the research grant #091019CRP2114 “Three-Dimensional All Solid State Rechargeable Batteries” from Nazarbayev University.

References

1 J. Y. Liao, D. Higgins, G. Lui, V. Chabot, X. Xiao and Z. Chen, Multifunctional TiO_2-C/MnO_2 core-double-shell nanowire arrays as high-performance 3D electrodes for lithium ion batteries, *Nano Lett.*, 2013, **13**, 5467–5473, DOI: **10.1021/nl4030159**.

2 F. M. Hassan, Z. Chen, A. Yu, Z. Chen and X. Xiao, Sn/SnO_2 embedded in mesoporous carbon nanocomposites as negative electrode for lithium ion batteries, *Electrochim. Acta*, 2013, **87**, 844–852, DOI: **10.1016/j.electacta.2012.09.015**.

3 N. Liu, H. Wu, M. T. McDowell, Y. Yao, C. Wang and Y. Cui, A yolk–shell design for stabilized and scalable Li-ion battery alloy anodes, *Nano Lett.*, 2012, **12**, 3315–3321, DOI: **10.1021/nl3014814**.

4 S. Ni, S. Tan, Q. An and L. Mai, Three dimensional porous frameworks for lithium dendrite suppression, *J. Energy Chem.*, 2020, **44**, 73–89, DOI: **10.1016/j.jechem.2019.09.031**.

5 H. Lee, J. Song, Y. J. Kim, J. K. Park and H. T. Kim, Structural modulation of lithium metal-electrolyte interface with three-dimensional metallic interlayer for high-performance lithium metal batteries, *Sci. Rep.*, 2016, **6**, 1–10, DOI: **10.1038/srep30830**.

6 T. S. Arthur, D. J. Bates, N. Cirigliano, D. C. Johnson, P. Malati, J. M. Mosby, E. Perre, M. T. Rawls, A. L. Prieto and B. Dunn, Three-dimensional electrodes and battery architectures, *MRS Bull.*, 2011, **36**, 523–531, DOI: **10.1557/mrs.2011.156**.

7 X. B. Cheng, T. Z. Hou, R. Zhang, H. J. Peng, C. Z. Zhao, J. Q. Huang and Q. Zhang, Dendrite-Free Lithium Deposition Induced by Uniformly Distributed Lithium Ions

for Efficient Lithium Metal Batteries, *Adv. Mater.*, 2016, **28**, 2888–2895, DOI: 10.1002/adma.201506124.

8 A. Mejía, S. Devaraj, J. Guzmán, J. M. Lopez Del Amo, N. García, T. Rojo, M. Armand and P. Tiemblo, Scalable plasticized polymer electrolytes reinforced with surface-modified sepiolite fillers – a feasibility study in lithium metal polymer batteries, *J. Power Sources*, 2016, **306**, 772–778, DOI: 10.1016/j.jpowsour.2015.12.099.

9 S. Kalybekkyzy, A. F. Kopzhassar, M. V. Kahraman, A. Mentbayeva and Z. Bakenov, Fabrication of UV-crosslinked flexible solid polymer electrolyte with PDMS for li-ion batteries, *Polymers*, 2021, **23**, 1–12, DOI: 10.3390/polym13010015.

10 N. Tolganbek, A. Mentbayeva, B. Uzakbaiuly, K. Kanamura and Z. Bakenov, $Li_{1+x}Al_xTi_{2-x}(PO_4)_3$, NASICON-type solid electrolyte fabrication with different methods, *Mater. Today Proc.*, 2019, **25**, 97–100, DOI: 10.1016/j.matpr.2019.12.279.

11 R. C. Agrawal and G. P. Pandey, Solid polymer electrolytes: materials designing and all-solid-state battery applications: an overview, *J. Phys. D: Appl. Phys.*, 2008, **41**, 1–18, DOI: 10.1088/0022-3727/41/22/223001.

12 G. El-Enany, M. J. Lacey, P. A. Johns and J. R. Owen, In situ growth of polymer electrolytes on lithium ion electrode surfaces, *Electrochem. Commun.*, 2009, **11**, 2320–2323, DOI: 10.1016/j.elecom.2009.10.019.

13 J. Xiang, Y. Zhao, L. Yuan, C. Chen, Y. Shen, F. Hu, Z. Hao, J. Liu, B. Xu and Y. Huang, A strategy of selective and dendrite-free lithium deposition for lithium batteries, *Nano Energy*, 2017, **42**, 262–268, DOI: 10.1016/j.nanoen.2017.10.065.

14 K. Yoo, A. Deshpande, S. Banerjee and P. Dutta, Electrochemical Model for Ionic Liquid Electrolytes in Lithium Batteries, *Electrochim. Acta*, 2015, **176**, 301–310, DOI: 10.1016/j.electacta.2015.07.003.

15 M. Montanino, M. Moreno, M. Carewska, G. Maresca, E. Simonetti, R. Lo Presti, F. Alessandrini and G. B. Appetecchi, Mixed organic compound-ionic liquid electrolytes for lithium battery electrolyte systems, *J. Power Sources*, 2014, **269**, 608–615, DOI: 10.1016/j.jpowsour.2014.07.027.

16 S. Xiong, J. Scheers, L. Aguilera, D. H. Lim, K. Xie, P. Jacobsson and A. Matic, Role of organic solvent addition to ionic liquid electrolytes for lithium-sulphur batteries, *RSC Adv.*, 2015, **5**, 2122–2128, DOI: 10.1039/c4ra14824j.

17 Y. Chen, K. Wen, T. Chen, X. Zhang, M. Armand and S. Chen, Recent progress in all-solid-state lithium batteries: the emerging strategies for advanced electrolytes and their interfaces, *Energy Stor. Mater.*, 2020, **31**, 401–433, DOI: 10.1016/j.ensm.2020.05.019.

18 Y. Zheng, Y. Yao, J. Ou, M. Li, D. Luo, H. Dou, Z. Li, K. Amine, A. Yu and Z. Chen, A review of composite solid-state electrolytes for lithium batteries: fundamentals, key materials and advanced structures, *Chem. Soc. Rev.*, 2020, **49**, 8790–8839, DOI: 10.1039/d0cs00305k.

19 K. Xu, Nonaqueous liquid electrolytes for lithium-based rechargeable batteries, *Chem. Rev.*, 2004, **104**, 4303–4417, DOI: 10.1021/cr030203g.

20 B. Zhang, R. Tan, L. Yang, J. Zheng, K. Zhang, S. Mo, Z. Lin and F. Pan, Mechanisms and properties of ion-transport in inorganic solid electrolytes, *Energy Stor. Mater.*, 2018, **10**, 139–159, DOI: 10.1016/j.ensm.2017.08.015.

21 F. Zheng, M. Kotobuki, S. Song, M. O. Lai and L. Lu, Review on solid electrolytes for all-solid-state lithium-ion batteries, *J. Power Sources*, 2018, **389**, 198–213, DOI: 10.1016/j.jpowsour.2018.04.022.

22 J. Hassoun, R. Verrelli, P. Reale, S. Panero, G. Mariotto, S. Greenbaum and B. Scrosati, A structural, spectroscopic and electrochemical study of a lithium ion conducting $Li_{10}GeP_2S_{12}$ solid electrolyte, *J. Power Sources*, 2013, **229**, 117–122, DOI: 10.1016/j.jpowsour.2012.11.130.

23 T. Šalkus, A. Dindune, Z. Kanepe, J. Ronis, A. Určinskas, A. Kežionis and A. F. Orliukas, Lithium ion conductors in the system $Li_{1+y}Ge_{2-x-y}Ti_xAl_y(PO_4)_3$ ($x = 0.1 \div 0.3$, $y = 0.07 \div 0.21$), *Solid State Ionics*, 2007, **178**, 1282–1287, DOI: 10.1016/j.ssi.2007.07.002.

24 W. J. Li, M. Hirayama, K. Suzuki and R. Kanno, Fabrication and electrochemical properties of a $LiCoO_2$ and $Li_{10}GeP_2S_{12}$ composite electrode for use in all-solid-state batteries, *Solid State Ionics*, 2016, **285**, 136–142, DOI: 10.1016/j.ssi.2015.05.007.

25 H. Aono, N. Imanaka and G. ya Adachi, High Li^+ Conducting Ceramics, *Acc. Chem. Res.*, 1994, **27**, 265–270, DOI: 10.1021/ar00045a002.

26 V. Thangadurai, A. K. Shukla and J. Gopalakrishnan, LiSr1.650.35B1.3B′ 1.7O9 (B = Ti, Zr; B′ = Nb, Ta): new lithium ion conductors based on the perovskite structure, *Chem. Mater.*, 1999, **11**, 835–839, DOI: 10.1021/cm9810382.

27 A. Karthikeyan, P. Vinatier and A. Levasseur, Study of lithium glassy solid electrolyte/electrode interface by impedance analysis, *Bull. Mater. Sci.*, 2000, **23**, 179–183, DOI: 10.1007/BF02719906.

28 F. Bai, K. Kakimoto, X. Shang, D. Mori, S. Taminato, M. Matsumoto, Y. Takeda, O. Yamamoto, H. Izumi, H. Minami and N. Imanishi, Water-Stable High Lithium-Ion Conducting Solid Electrolyte of $Li_{1.4}Al_{0.4}Ge_{0.2}Ti_{1.4}(PO_4)_3$–LiCl for Aqueous Lithium-Air Batteries, *Front. Energy Res.*, 2020, **8**, 2–10, DOI: 10.3389/fenrg.2020.00187.

29 H. Chung and B. Kang, Mechanical and Thermal Failure Induced by Contact between a $Li_{1.5}Al_{0.5}Ge_{1.5}(PO_4)_3$ Solid Electrolyte and Li Metal in an All Solid-State Li Cell, *Chem. Mater.*, 2017, **29**, 8611–8619, DOI: 10.1021/acs.chemmater.7b02301.

30 A. Martínez-Juárez, C. Pecharromán, J. E. Iglesias and J. M. Rojo, Relationship between activation energy and bottleneck size for Li^+ ion conduction in NASICON materials of composition $LiMM'(PO_4)_3$; M, M′ = Ge, Ti, Sn, Hf, *J. Phys. Chem. B*, 1998, **102**, 372–375, DOI: 10.1021/jp973296c.

31 T. Krauskopf, S. P. Culver and W. G. Zeier, Bottleneck of Diffusion and Inductive Effects in $Li_{10}Ge_{1-x}Sn_xP_2S_{12}$, *Chem. Mater.*, 2018, **30**, 1791–1798, DOI: 10.1021/acs.chemmater.8b00266.

32 J. Liu, T. Liu, Y. Pu, M. Guan, Z. Tang, F. Ding, Z. Xu and Y. Li, Facile synthesis of NASICON-type $Li_{1.3}Al_{0.3}Ti_{1.7}(PO_4)_3$ solid electrolyte and its application for enhanced cyclic performance in lithium ion batteries through the introduction of an artificial Li_3PO_4 SEI layer, *RSC Adv.*, 2017, **7**, 46545–46552, DOI: **10.1039/C7RA09335G**.

33 L. Li, Z. Zhang, L. Luo, R. You, J. Jiao, W. Huang, J. Wang, C. Li, X. Han and S. Chen, Enhancing the interface stability of $Li_{1.3}Al_{0.3}Ti_{1.7}(PO_4)_3$ and lithium metal by amorphous $Li_{1.5}Al_{0.5}Ge_{1.5}(PO_4)_3$ modification, *Ionics*, 2020, **26**, 3815–3821, DOI: **10.1007/s11581-020-03503-x**.

34 S. Xiong, Y. Liu, P. Jankowski, Q. Liu, F. Nitze, K. Xie, J. Song and A. Matic, Design of a Multifunctional Interlayer for NASCION-Based Solid-State Li Metal Batteries, *Adv. Funct. Mater.*, 2020, **30**, 1–10, DOI: **10.1002/adfm.20201444**.

35 Y. Meesala, A. Jena, H. Chang and R. S. Liu, Recent Advancements in Li-Ion Conductors for All-Solid-State Li-Ion Batteries, *ACS Energy Lett.*, 2017, **2**, 2734–2751, DOI: **10.1021/acsenergylett.7b00849**.

36 J. C. Bachman, S. Muy, A. Grimaud, H. H. Chang, N. Pour, S. F. Lux, O. Paschos, F. Maglia, S. Lupart, P. Lamp, L. Giordano and Y. Shao-Horn, Inorganic Solid-State Electrolytes for Lithium Batteries: Mechanisms and Properties Governing Ion Conduction, *Chem. Rev.*, 2016, **116**, 140–162, DOI: **10.1021/acs.chemrev.5b00563**.

37 H. Aono, E. Sugimoto, Y. Sadaoka, N. Imanaka and G. Adachi, Electrical Properties and Sinterability for Lithium Germanium Phosphate $Li_{1+x}M_xGe_{2-x}(PO_4)_3$, M = Al, Cr, Ga, Fe, Sc, and In Systems, *Bull. Chem. Soc. Jpn.*, 1992, **65**, 2200–2204, DOI: **10.1246/bcsj.65.2200**.

38 S. Chun Li, J. Yi Cai and Z. Xiang Lin, Phase relationships and electrical conductivity of $Li_{1+x}Ge_{2-x}Al_xP_3O_{12}$ and $Li_{1+x}Ge_{2-x}Cr_xP_3O_{12}$ systems, *Solid State Ionics*, 1988, **28–30**, 1265–1270, DOI: **10.1016/0167-2738(88)90368-2**.

39 M. Kotobuki and M. Koishi, Preparation of $Li_{1.5}Al_{0.5}Ti_{1.5}(PO_4)_3$ solid electrolyte via a sol-gel route using various Al sources, *Ceram. Int.*, 2013, **39**, 4645–4649, DOI: **10.1016/j.ceramint.2012.10.206**.

40 Z. Yang, H. Yuan, C. Zhou, Y. Wu, W. Tang, S. Sang and H. Liu, Facile interfacial adhesion enabled LATP-based solid-state lithium metal battery, *Chem. Eng. J.*, 2020, **392**, 123650, DOI: **10.1016/j.cej.2019.123650**.

41 B. Yang, X. Li, H. Guo, Z. Wang and W. Xiao, Preparation and properties of $Li_{1.3}Al_{0.3}Ti_{1.7}(PO_4)_3$ by spray-drying and post-calcining method, *J. Alloys Compd.*, 2015, **643**, 181–185, DOI: **10.1016/j.jallcom.2015.04.019**.

42 J. Liu, T. Liu, Y. Pu, M. Guan, Z. Tang, F. Ding, Z. Xu and Y. Li, Facile synthesis of NASICON-type $Li_{1.3}Al_{0.3}Ti_{1.7}(PO_4)_3$ solid electrolyte and its application for enhanced cyclic performance in lithium ion batteries through the introduction of an artificial Li_3PO_4 SEI layer, *RSC Adv.*, 2017, **7**, 46545–46552, DOI: **10.1039/c7ra09335g**.

43 M. Monchak, T. Hupfer, A. Senyshyn, H. Boysen, D. Chernyshov, T. Hansen, K. G. Schell, E. C. Bucharsky, M. J. Hoffmann and H. Ehrenberg, Lithium Diffusion Pathway in $Li_{1.3}Al_{0.3}Ti_{1.7}(PO_4)_3$ (LATP) Superionic Conductor, *Inorg. Chem.*, 2016, **55**, 2941–2945, DOI: **10.1021/acs.inorgchem.5b02821**.

44 X. Liang, D. Han, Y. Wang, L. Lan and J. Mao, Preparation and performance study of a PVDF-LATP ceramic composite polymer electrolyte membrane for solid-state batteries, *RSC Adv.*, 2018, **8**, 40498–40504, DOI: **10.1039/C8RA08436J**.

45 E. Zhao, F. Ma, Y. Jin and K. Kanamura, Pechini synthesis of high ionic conductivity $Li_{1.3}Al_{0.3}Ti_{1.7}(PO_4)_3$ solid electrolytes: the effect of dispersant, *J. Alloys Compd.*, 2016, **680**, 646–653, DOI: **10.1016/j.jallcom.2016.04.173**.

46 L. Ti, A. Po, M. Schroeder, S. Glatthaar and J. R. Binder, In fluence of spray granulation on the properties of wet chemically synthesized, *Solid State Ionics*, 2011, **201**, 49–53, DOI: **10.1016/j.ssi.2011.08.014**.

47 H. Morimoto, H. Awano, J. Terashima and Y. Shindo, Preparation of lithium ion conducting solid electrolyte of NASICON-type obtained by using the mechanochemical method and its application as surface modi fi cation materials of $LiCoO_2$ cathode for lithium cell, *J. Power Sources*, 2013, **240**, 636–643, DOI: **10.1016/j.jpowsour.2013.05.039**.

48 F. Ma, E. Zhao, S. Zhu, W. Yan, D. Sun, Y. Jin and C. Nan, Preparation and evaluation of high lithium ion conductivity $Li_{1.3}Al_{0.3}Ti_{1.7}(PO_4)_3$ solid electrolyte obtained using a new solution method, *Solid State Ionics*, 2016, **295**, 7–12, DOI: **10.1016/j.ssi.2016.07.010**.

49 M. D. Singh, A. Dalvi, D. M. Phase and Y. Kumar, $Li_{1.3}Al_{0.3}Ti_{1.7}(PO_4)_3$ reinforced hybrid polymer composites: assessment of enhanced Li^+ ion transport and potential for solid-state supercapacitor applications, *J. Mater. Sci.*, 2020, **55**, 3951–3963, DOI: **10.1007/s10853-019-04234-9**.

50 W. Zhou, S. Wang, Y. Li, S. Xin, A. Manthiram and J. B. Goodenough, Plating a Dendrite-Free Lithium Anode with a Polymer/Ceramic/Polymer Sandwich Electrolyte, *J. Am. Chem. Soc.*, 2016, **138**, 9385–9388, DOI: **10.1021/jacs.6b05341**.

51 Y. S. Lim, H. A. Jung and H. Hwang, Fabrication of PEO-PMMA-$LiClO_4$-Based Solid Polymer Electrolytes Containing Silica Aerogel Particles for All-Solid-State Lithium Batteries, *Energies*, 2018, **11**, 1–10, DOI: **10.3390/en11102559**.

52 X. Shi, N. Ma, Y. Wu, Y. Lu, Q. Xiao, Z. Li and G. Lei, Fabrication and electrochemical properties of LATP/PVDF composite electrolytes for rechargeable lithium-ion battery, *Solid State Ionics*, 2018, **325**, 112–119, DOI: **10.1016/j.ssi.2018.08.010**.

53 X. Song, H. Zhang, D. Jiang, L. Yang, J. Zhang, M. Yao, X. Ji, G. Wang and S. Zhang, Enhanced transport and favorable distribution of Li-ion in a poly(ionic liquid) based electrolyte facilitated by $Li_{1.3}Al_{0.3}Ti_{1.7}(PO_4)_3$ nanoparticles for highly-safe lithium metal batteries, *Electrochim. Acta*, 2021, **368**, 137581, DOI: **10.1016/j.electacta.2020.137581**.

54 R. F. Samsinger, S. O. Schopf, J. Schuhmacher, P. Treis, M. Schneider, A. Roters and A. Kwade, Influence of the Processing on the Ionic Conductivity of Solid-State Hybrid Electrolytes Based on Glass-Ceramic Particles Dispersed in PEO with LiTFSI, *J. Electrochem. Soc.*, 2020, **167**, 120538, DOI: **10.1149/1945-7111/abb37f**.

55 Z. Yao, K. Zhu, X. Li, J. Zhang, J. Li, J. Wang, K. Yan and J. Liu, Double-Layered Multifunctional Composite Electrolytes for High-Voltage Solid-State Lithium-Metal Batteries, *ACS Appl. Mater. Interfaces*, 2021, **13**, 11958–11967, DOI: **10.1021/acsami.0c22532**.

56 S. Yi, T. Xu, L. Li, M. Gao, K. Du, H. Zhao and Y. Bai, Fast ion conductor modified double-polymer (PVDF and PEO) matrix electrolyte for solid lithium-ion batteries, *Solid State Ionics*, 2020, **355**, 1–10, DOI: **10.1016/j.ssi.2020.115419**.

57 J. Y. Ock, M. Fujishiro, K. Ueno, I. Kawamura, R. Tatara, K. Hashimoto, M. Watanabe and K. Dokko, Transport Properties of Flexible Composite Electrolytes Composed of $Li_{1.5}Al_{0.5}Ti_{1.5}(PO_4)_3$ and a Poly(vinylidene fluoride-co-hexafluoropropylene) Gel Containing a Highly Concentrated $Li[N(SO_2CF_3)_2]$/Sulfolane Electrolyte, *ACS Omega*, 2021, **6**, 16187–16193, DOI: **10.1021/acsomega.1c02161**.

58 L. Yue, J. Ma, J. Zhang, J. Zhao, S. Dong, Z. Liu, G. Cui and L. Chen, All solid-state polymer electrolytes for high-performance lithium ion batteries, *Energy Stor. Mater.*, 2016, **5**, 139–164, DOI: **10.1016/j.ensm.2016.07.003**.

59 Q. Cheng, A. Li, N. Li, S. Li, A. Zangiabadi, T. De Li, W. Huang, A. C. Li, T. Jin, Q. Song, W. Xu, N. Ni, H. Zhai, M. Dontigny, K. Zaghib, X. Chuan, D. Su, K. Yan and Y. Yang, Stabilizing Solid Electrolyte-Anode Interface in Li-Metal Batteries by Boron Nitride-Based Nanocomposite Coating, *Joule*, 2019, **3**, 1510–1522, DOI: **10.1016/j.joule.2019.03.022**.

60 H. Bai, J. Hu, Y. Duan, T. Kozawa, M. Naito, J. Zhang and S. Dong, Surface modification of $Li_{1.3}Al_{0.3}Ti_{1.7}(PO_4)_3$ ceramic electrolyte by Al_2O_3-doped ZnO coating to enable dendrites-free all-solid-state lithium-metal batteries, *Ceram. Int.*, 2019, **45**, 14663–14668, DOI: **10.1016/j.ceramint.2019.04.185**.

61 X. Hao, Q. Zhao, S. Su, S. Zhang, J. Ma, L. Shen, Q. Yu, L. Zhao, Y. Liu, F. Kang and Y. B. He, Constructing Multifunctional Interphase between $Li_{1.4}Al_{0.4}Ti_{1.6}(PO_4)_3$ and Li Metal by Magnetron Sputtering for Highly Stable Solid-State Lithium Metal Batteries, *Adv. Energy Mater.*, 2019, **9**, 1–8, DOI: **10.1002/aenm.201901604**.

62 Y. Liu, C. Li, B. Li, H. Song, Z. Cheng, M. Chen, P. He and H. Zhou, Germanium Thin Film Protected Lithium Aluminum Germanium Phosphate for Solid-State Li Batteries, *Adv. Energy Mater.*, 2018, **8**, 1–7, DOI: **10.1002/aenm.201702374**.

63 Y. Hu, Y. Zhong, L. Qi and H. Wang, Inorganic/polymer hybrid layer stabilizing anode/electrolyte interfaces in solid-state Li metal batteries, *Nano Res.*, 2020, **13**, 3230–3234, DOI: **10.1007/s12274-020-2993-4**.

64 Y. Kee, Y. Suzuki, N. Ishigaki, M. Motoyama, Y. Kimura, K. Amezawa and Y. Iriyama, An appropriate reference and counter electrode in an all-solid-state battery using NASICON-structured solid electrolyte, *Electrochem. Commun.*, 2021, **130**, 107108, DOI: **10.1016/j.elecom.2021.107108**.

65 N. W. Li, Y. X. Yin, C. P. Yang and Y. G. Guo, An Artificial Solid Electrolyte Interphase Layer for Stable Lithium Metal Anodes, *Adv. Mater.*, 2016, **28**, 1853–1858, DOI: **10.1002/adma.201504526**.

66 Y. Liu, Q. Sun, Y. Zhao, B. Wang, P. Kaghazchi, K. R. Adair, R. Li, C. Zhang, J. Liu, L. Y. Kuo, Y. Hu, T. K. Sham, L. Zhang, R. Yang, S. Lu, X. Song and X. Sun, Stabilizing the Interface of NASICON Solid Electrolyte against Li Metal with Atomic Layer Deposition, *ACS Appl. Mater. Interfaces*, 2018, **10**, 31240–31248, DOI: **10.1021/acsami.8b06366**.

67 L. Yang, Y. Song, H. Liu, Z. Wang, K. Yang, Q. Zhao, Y. Cui, J. Wen, W. Luo and F. Pan, Stable Interface between Lithium and Electrolyte Facilitated by a Nanocomposite Protective Layer, *Small Methods*, 2020, **4**, 1–7, DOI: **10.1002/smtd.201900751**.

68 Z. Y. Kou, Y. Lu, C. Miao, J. Q. Li, C. J. Liu and W. Xiao, High-performance sandwiched hybrid solid electrolytes by coating polymer layers for all-solid-state lithium-ion batteries, *Rare Met.*, 2021, **40**, 3175–3184, DOI: **10.1007/s12598-020-01678-w**.

69 L. He, Q. Sun, C. Chen, J. A. S. Oh, J. Sun, M. Li, W. Tu, H. Zhou, K. Zeng and L. Lu, Failure Mechanism and Interface Engineering for NASICON-Structured All-Solid-State Lithium Metal Batteries, *ACS Appl. Mater. Interfaces*, 2019, **11**, 20895–20904, DOI: **10.1021/acsami.9b05516**.

70 Y. Wang, G. Wang, P. He, J. Hu, J. Jiang and L. Z. Fan, Sandwich structured NASICON-type electrolyte matched with sulfurized polyacrylonitrile cathode for high performance solid-state lithium-sulfur batteries, *Chem. Eng. J.*, 2020, **393**, 124705, DOI: **10.1016/j.cej.2020.124705**.

71 X. Yu and A. Manthiram, Enhanced Interfacial Stability of Hybrid-Electrolyte Lithium-Sulfur Batteries with a Layer of Multifunctional Polymer with Intrinsic Nanoporosity, *Adv. Funct. Mater.*, 2019, **29**, 1–10, DOI: **10.1002/adfm.201805996**.

72 Z. Chen, G. T. Kim, J. K. Kim, M. Zarrabeitia, M. Kuenzel, H. P. Liang, D. Geiger, U. Kaiser and S. Passerini, Highly Stable Quasi-Solid-State Lithium Metal Batteries: Reinforced $Li_{1.3}Al_{0.3}Ti_{1.7}(PO_4)_3$/Li Interface by a Protection Interlayer, *Adv. Energy Mater.*, 2021, **11**, 1–16, DOI: **10.1002/aenm.202101339**.

73 Y. Koizumi, D. Mori, S. Taminato, O. Yamamoto, Y. Takeda and N. Imanishi, Lithium-stable NASICON-type lithium-ion conducting solid electrolyte film coated with a polymer electrolyte, *Solid State Ionics*, 2019, **337**, 101–106, DOI: **10.1016/j.ssi.2019.04.016**.

74 Z. Cai, R. Xiao and B. Jiang, Architecting with a flexible and modified polyethylene oxide coating for ambient-temperature solid-state Li metal batteries, *Surf. Coat. Technol.*, 2021, **421**, 127389, DOI: **10.1016/j.surfcoat.2021.127389**.

75 Y. Jin, C. Liu, X. Zong, D. Li, M. Fu, S. Tan, Y. Xiong and J. Wei, Multifunctional Interfacial Layer for All-Solid-State Lithium Batteries, *J. Power Sources*, 2020, **460**, 228125, DOI: **10.1016/j.jpowsour.2020.228125**.

76 S. Yu, S. Schmohl, Z. Liu, M. Hoffmeyer, N. Schön, F. Hausen, H. Tempel, H. Kungl, H. D. Wiemhöfer and R. A. Eichel, Insights into a layered hybrid solid electrolyte and its application in long lifespan high-voltage all-solid-

state lithium batteries, *J. Mater. Chem. A.*, 2019, **7**, 3882–3894, DOI: **10.1039/c8ta11259b**.

77 C. Guhl, M. Fingerle and R. Hausbrand, Process related effects upon formation of composite electrolyte interfaces: nitridation and reduction of NASICON-type electrolytes by deposition of LiPON, *J. Power Sources*, 2017, **362**, 299–307, DOI: **10.1016/j.jpowsour.2017.07.051**.

78 F. J. Q. Cortes, J. A. Lewis, J. Tippens, T. S. Marchese and M. T. McDowell, How Metallic Protection Layers Extend the Lifetime of NASICON-Based Solid-State Lithium Batteries, *J. Electrochem. Soc.*, 2020, **167**, 050502, DOI: **10.1149/2.0032005jes**.

79 N. Tolganbek, A. Serikkazyyeva, S. Kalybekkyzy, M. Sarsembina, K. Kanamura, Z. Bakenov and A. Mentbayeva, Interface modification of NASICON-type Li-ion conducting ceramic electrolytes: a critical evaluation, *Mater. Adv.*, 2022, **3**, 3055–3069, DOI: **10.1039/d1ma01239h**.

80 N. Tolganbek, Y. Yerkinbekova, A. Khairullin, Z. Bakenov, K. Kanamura and A. Mentbayeva, Enhancing purity and ionic conductivity of NASICON-typed $Li_{1.3}Al_{0.3}Ti_{1.7}(PO_4)_3$ solid electrolyte, *Ceram. Int.*, 2021, **47**, 18188–18195, DOI: **10.1016/j.ceramint.2021.03.137**.

81 N. Tolganbek, A. Mentbayeva, N. Serik, N. Batyrgali, M. Naizakarayev, K. Kanamura and Z. Bakenov, Design and preparation of thin film gel polymer electrolyte for 3D Li-ion battery, *J. Power Sources*, 2021, **493**, 229686, DOI: **10.1016/j.jpowsour.2021.229686**.

82 A. Mentbayeva, S. Sukhishvili, M. Naizakarayev and N. Batyrgali, Electrochimica Acta Ultrathin clay-containing layer-by-layer separator coating enhances performance of lithium-sulfur batteries, *Electrochim. Acta*, 2021, **366**, 137454, DOI: **10.1016/j.electacta.2020.137454**.

83 Z. Wang, L. Ouyang, H. Li, L. Wågberg and M. M. Hamedi, Layer-by-Layer Assembly of Strong Thin Films with High Lithium Ion Conductance for Batteries and Beyond, *Small*, 2021, **17**, 1–7, DOI: **10.1002/smll.202100954**.

84 J. Zhu, J. Zhao, Y. Xiang, M. Lin, H. Wang, B. Zheng, H. He, Q. Wu, J. Y. Huang and Y. Yang, Chemomechanical Failure Mechanism Study in NASICON-Type $Li_{1.3}Al_{0.3}Ti_{1.7}(PO_4)_3$ Solid-State Lithium Batteries, *Chem. Mater.*, 2020, **32**, 4998–5008, DOI: **10.1021/acs.chemmater.9b05295**.

85 X. B. Cheng, C. Z. Zhao, Y. X. Yao, H. Liu and Q. Zhang, Recent Advances in Energy Chemistry between Solid-State Electrolyte and Safe Lithium-Metal Anodes, *Chem*, 2019, **5**, 74–96, DOI: **10.1016/j.chempr.2018.12.002**.

86 A. Jena, Y. Meesala, S. F. Hu, H. Chang and R. S. Liu, Ameliorating interfacial ionic transportation in all-solid-state li-ion batteries with interlayer modifications, *ACS Energy Lett.*, 2018, **3**, 2775–2795, DOI: **10.1021/acsenergylett.8b01564**.

87 D. M. Delongchamp and P. T. Hammond, Highly ion conductive poly(ethylene oxide)-based solid polymer electrolytes from hydrogen bonding layer-by-layer assembly, *Langmuir*, 2004, **20**, 5403–5411, DOI: **10.1021/la049777m**.

88 Z. Yang, H. Yuan, C. Zhou, Y. Wu, W. Tang, S. Sang and H. Liu, Facile interfacial adhesion enabled LATP-based solid-state lithium metal battery, *Chem. Eng. J.*, 2020, **392**, 123650, DOI: **10.1016/j.cej.2019.123650**.

89 X. Ke, Y. Wang, L. Dai and C. Yuan, Cell failures of all-solid-state lithium metal batteries with inorganic solid electrolytes: Lithium dendrites, *Energy Stor. Mater.*, 2020, **33**, 309–328, DOI: **10.1016/j.ensm.2020.07.024**.

90 M. Diaz, *Nano-scale mechanism of crack nucleation/propagation and lithium penetration in solid electrolyte*, 2022.

91 M. B. Dixit, A. Verma, W. Zaman, X. Zhong, P. Kenesei, J. S. Park, J. Almer, P. P. Mukherjee and K. B. Hatzell, Synchrotron imaging of pore formation in Li metal solid-state batteries aided by machine learning, *ACS Appl. Energy Mater.*, 2020, **3**, 9534–9542, DOI: **10.1021/acsaem.0c02053**.

92 M. B. Dixit, N. Singh, J. P. Horwath, P. D. Shevchenko, M. Jones, E. A. Stach, T. S. Arthur and K. B. Hatzell, In Situ Investigation of Chemomechanical Effects in Thiophosphate Solid Electrolytes, *Matter*, 2020, **3**, 2138–2159, DOI: **10.1016/j.matt.2020.09.018**.

93 A. Mistry and P. P. Mukherjee, Molar Volume Mismatch: A Malefactor for Irregular Metallic Electrodeposition with Solid Electrolytes, *J. Electrochem. Soc.*, 2020, **167**, 082510, DOI: **10.1149/1945-7111/ab8ecd**.

94 L. Porz, T. Swamy, B. W. Sheldon, D. Rettenwander, T. Frömling, H. L. Thaman, S. Berendts, R. Uecker, W. C. Carter and Y. M. Chiang, Mechanism of Lithium Metal Penetration through Inorganic Solid Electrolytes, *Adv. Energy Mater.*, 2017, **7**, 1–12, DOI: **10.1002/aenm.201701003**.

95 J. Tippens, J. C. Miers, A. Afshar, J. A. Lewis, F. J. Q. Cortes, H. Qiao, T. S. Marchese, C. V. Di Leo, C. Saldana and M. T. McDowell, Visualizing Chemomechanical Degradation of a Solid-State Battery Electrolyte, *ACS Energy Lett.*, 2019, **4**, 1475–1483, DOI: **10.1021/acsenergylett.9b00816**.

96 E. Kazyak, R. Garcia-Mendez, W. S. LePage, A. Sharafi, A. L. Davis, A. J. Sanchez, K. H. Chen, C. Haslam, J. Sakamoto and N. P. Dasgupta, Li Penetration in Ceramic Solid Electrolytes: Operando Microscopy Analysis of Morphology, Propagation, and Reversibility, *Matter*, 2020, **2**, 1025–1048, DOI: **10.1016/j.matt.2020.02.008**.

97 C. Fu, V. Venturi, J. Kim, Z. Ahmad, A. W. Ells, V. Viswanathan and B. A. Helms, Universal chemomechanical design rules for solid-ion conductors to prevent dendrite formation in lithium metal batteries, *Nat. Mater.*, 2020, **19**, 758–766, DOI: **10.1038/s41563-020-0655-2**.

98 A. Sharafi, H. M. Meyer, J. Nanda, J. Wolfenstine and J. Sakamoto, Characterizing the Li-$Li_7La_3Zr_2O_{12}$ interface stability and kinetics as a function of temperature and current density, *J. Power Sources*, 2016, **302**, 135–139, DOI: **10.1016/j.jpowsour.2015.10.053**.